EFFECT OF WORKING-FLUID MIXTURES ON ORGANIC RANKINE CYCLE SYSTEM PERFORMANCE: HEAT TRANSFER AND COST ANALYSIS

Oyewunmi O.A. and Markides C.N.*
*Author for correspondence
Clean Energy Processes (CEP) Laboratory, Chemical Engineering Department, Imperial College London,
London SW7 2AZ, United Kingdom,
E-mail: c.markides@imperial.ac.uk

ABSTRACT

A thermodynamic limitation of single-component working fluids in organic Rankine cycles (ORCs) is the large exergy destruction (and, consequently, useful power loss) associated with evaporation and condensation. Due to their non-isothermal phase-change behaviour, non-azeotropic working-fluid mixtures have shown reduced exergy losses, leading to improved cycle efficiencies and power outputs. These benefits are exclusively observed from a thermodynamic perspective. The present paper considers the effects of selecting such working-fluid mixtures on heat transfer performance, component sizing and system costs compared with those of pure fluids; a mixture of *n*-pentane and *n*-hexane is selected. While the fluid-mixture cycles do indeed allow higher efficiencies and the generation of higher power outputs, they require larger evaporators, condensers and expanders; thus, the resulting ORC systems are more expensive than those based on the pure fluids. While a working-fluid mixture (60% *n*-pentane + 40% *n*-hexane) leads to the thermodynamically optimal cycle, a pure *n*-pentane ORC system has reduced costs of 37% per unit power output over the thermodynamic optimum.

INTRODUCTION

Recently, the selection of working fluids for organic Rankine cycles (ORCs) has received close attention, including a particular interest in multi-component fluid mixtures, due to the opportunities they offer in improving the thermodynamic performance of ORC systems. Various authors have carried out investigations to demonstrate and quantify these benefits, which have shown that working-fluid mixtures can exhibit an improved thermal match with the heat source compared to the isothermal evaporation profile of (isobaric) single-component fluids, resulting in reduced exergy destruction [1,2], and increased thermal and exergy efficiencies [3,4].

Various other authors have carried out both experimental and theoretical investigations into the benefits of employing refrigerant [5-10], hydrocarbon [9-13], and siloxane [1,14], working-fluid mixtures. Compared to pure fluids, suitable binary mixtures were shown increased power outputs by about 30% and thermal efficiencies by over 15%. Additionally, fluid mixtures can be used to adjust environmental and safety-related properties of the working fluid or to improve design parameters of cycle components [2]. However, some exceptions to these general trends have also been identified [15,16]. At the same time, a few investigators have begun to develop and employ advanced computer-aided molecular design (CAMD) methodologies [16-19] to identify optimal mixtures for ORCs.

While these efforts have demonstrated the potential advantages of working-fluid mixtures, notably in terms of power output and efficiency, many of the associated conclusions have been derived strictly based on thermodynamic cycle analyses that do not fully consider the expected heat transfer performance between the heat source/sink and working-fluid streams in the heat exchangers of ORC engines. In particular, the heat transfer and cost implications of using fluid mixtures have not been properly addressed. Refrigerant mixtures are known to exhibit reduced heat-transfer coefficients compared to their pure counterparts [20,21]. Specifically, heat-transfer coefficients for refrigerants mixtures are usually lower than the ideal values interpolated between the mixture components. This may invariably lead to larger and more expensive heat exchangers in an ORC system. Therefore, although working-fluid mixtures may allow a thermodynamic advantage over single-component working fluids, they may also lead to higher system costs owing to deterioration in their thermal performance.

This work aims to explore the effects of working-fluid mixtures on the heat transfer processes in ORC engines, which is important in understanding the role that these fluids play on the overall system performance and cost. A simple ORC engine model is presented that incorporates a heat transfer description of the heat exchangers used for the heat addition and heat rejection processes. The heat exchangers are discretized along their lengths into segments (accounting for phase-change and single-phase regions), with suitable estimates of the heat-transfer coefficients for the different segments. Overall heat-transfer coefficients and heat-transfer areas are then evaluated, and simple cost models are used to estimate the relative costs of the components, and by extension of the entire engine. Using a selection of alkane working-fluid mixtures, the heat transfer characteristics and ORC-system equipment/component costs are thus investigated.

ORC THERMODYNAMIC OPTIMIZATION

Following an approach similar to previous studies, we carry out a simple thermodynamic optimization of an ORC cycle with a set of working-fluid mixtures. In particular, we study straight-chained alkane mixtures of *n*-hexane and *n*-pentane. Pentane is presently being used in actual installations especially in geothermal ORC setups. Furthermore various authors [11-13] have shown that mixtures of these particular fluids can provide significant thermodynamic benefits to an ORC system.

ORC Model

A non-regenerative ORC, similarly to a steam-Rankine cycle, consists of four processes (pumping, heat addition, expansion and heat rejection), carried out by an organic working fluid. A typical such ORC is presented in the *T*-*s* diagram in Figure 1. The power required to pump the working fluid from State 1 to State 2 is:

$$\dot{W}_{\mathrm{pm}} = \dot{m}_{\mathrm{wf}}(h_2 - h_1) = \dot{m}_{\mathrm{wf}}(h_{2s} - h_1)/\eta_{\mathrm{is,pump}} \,. \quad [1]$$

The heat extracted from the heat source is transferred to the working fluid assuming no heat losses in the evaporator. This is assumed to be an isobaric process. The working fluid exits the evaporator as a saturated vapour as depicted in Figure 1. The working fluid is not superheated, since superheating has been shown to be detrimental to ORC performance [16]. Thus the rate of heat input from the heat source is given by:

$$\dot{Q}_{\mathrm{in}} = \dot{m}_{\mathrm{wf}}(h_3 - h_2) = \dot{m}_{\mathrm{hs}} c_{\mathrm{p,hs}} \left(T_{\mathrm{hs,in}} - T_{\mathrm{hs,out}}\right) . \quad [2]$$

The power generated as the working fluid is expanded is:

$$\dot{W}_{\mathrm{exp}} = \dot{m}_{\mathrm{wf}}(h_3 - h_4) = \eta_{\mathrm{is,exp}} \dot{m}_{\mathrm{wf}}(h_3 - h_{4s}) \,. \quad [3]$$

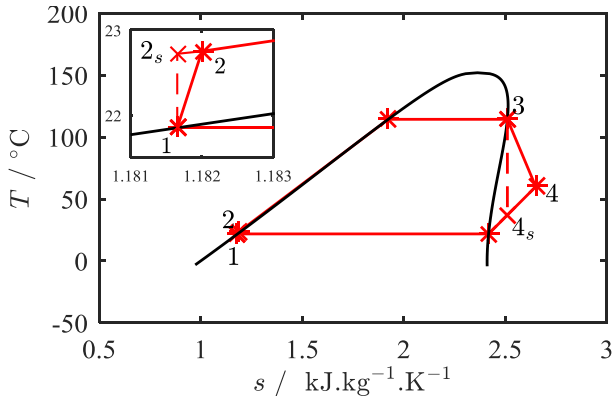

Figure 1: ORC *T-s* diagram for the case of a pure (single-component) working fluid

In the condenser, the working fluid rejects heat to a cooling stream (assuming no heat losses) at a rate given by:

$$\dot{Q}_{\text{out}} = \dot{m}_{\text{wf}}(h_4 - h_1) = \dot{m}_{\text{cs}} c_{p,\text{cs}} \left(T_{\text{cs,out}} - T_{\text{cs,in}}\right) . \quad [4]$$

The cycle thermal efficiency, η_{th}, is thus calculated as:

$$\eta_{\text{th}} = (\dot{W}_{\text{exp}} - \dot{W}_{\text{pump}}) / \dot{Q}_{\text{in}} . \quad [5]$$

Optimization Problem Definition

Multi-component working fluids are attractive in ORC systems owing to their non-isothermal phase-change processes during (isobaric) heat addition and rejection. This leads to a minimization of the average temperature difference between the heat source/sink and the working fluid and consequently to a reduction in exergy destruction in the heat exchangers.

A wide variety of heat-source streams can be used in ORC applications; these include thermal oil (*e.g.*, in solar applications), exhaust/flue gases, geothermal water *etc.* For the purpose of this work, it is more appropriate to consider liquid source and sink streams; employing a gaseous streams would dominate the thermal resistances on the source and sink side of the heat exchangers and thereby overshadow the resistances of the working-fluid vapour and liquid streams. This would consequently limit the information we hope to derive by employing different working-fluid mixtures. Thus, the heat source selected for the present work is a pressurized hot-water stream, typical of what is obtainable from geothermal reservoirs and from cooling streams in high temperature (and pressure) industrial processes. Similarly, the heat sink is a water stream at ambient conditions. The heat source and heat sink conditions are given in Table 1, which also includes other important ORC system parameters. The thermodynamic and transport properties of the working-fluid mixtures and the heat source and sink are calculated by using REFPROP 9.1 [22].

Table 1: ORC simulation parameters

Heat source		**Heat sink**	
$T_{\text{hs,in}}$	150 °C	$T_{\text{cs,in}}$	20 °C
$T_{\text{hs,out}}$	100 °C	$T_{\text{cs,out}}$	30 °C
$\dot{m}_{\text{hs}}$	50 kg.s^{-1}	$\eta_{\text{is,pump}}$, $\eta_{\text{is,exp}}$	75%

An optimization problem is thus set up to maximize the expansion power output ($\dot{W}_{\text{exp}}$) for the given heat source enthalpy flow and, concurrently, the overall cycle thermal efficiency. It should be noted that all the working-fluid mixtures are subjected to the same availability of thermal energy from the heat source in order to enable a uniform basis for comparison. The decision variables are the evaporation and condensation pressures, while the constraints are the pinch conditions (minimum of 10 °C) in the heat exchangers. We restrict our study to sub-critical cycles.

Optimal Cycles with Working-Fluid Mixtures

Using *n*-pentane + *n*-hexane mixtures (from pure *n*-pentane, $X_{\text{C6H14}} = 0$, to pure *n*-hexane, $X_{\text{C6H14}} = 1$, in steps of 0.1 mole fractions), the ORC is optimized for maximum $\dot{W}_{\text{exp}}$, using the Interior Point algorithm [23]. The optimal power output and associated operating pressures are presented in Figure 2, the evaporation and condensation temperature glides are presented in Figure 3, and other cycle parameters are presented in Table 2. The expander performance parameters (inlet/outlet volumetric flow-rates, pressure ratio and expansion ratio) are presented in Figure 4.

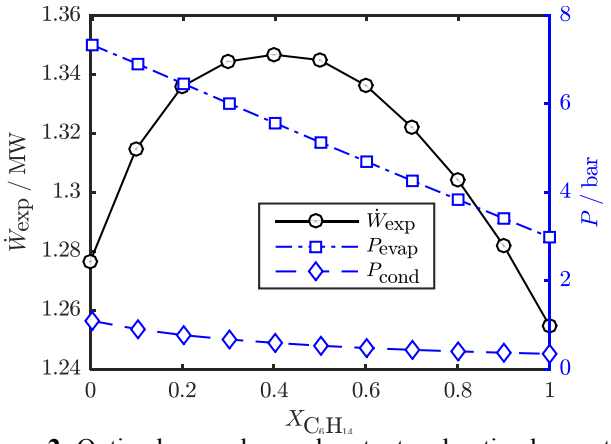

Figure 2: Optimal expander work output and optimal operating saturation-pressure conditions

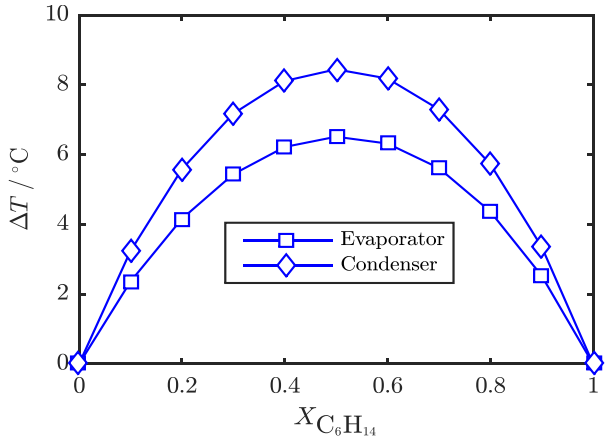

Figure 3: Evaporation and condensation temperature glides at optimal operating condition

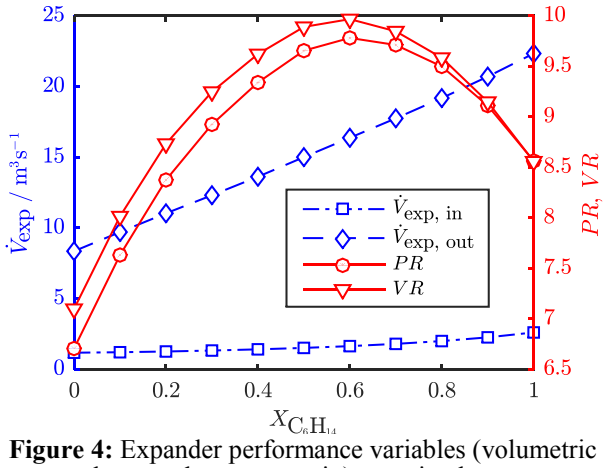

Figure 4: Expander performance variables (volumetric flow-rate, volume and pressure ratio) at optimal power output

Table 2: ORC optimization results

X_{C6H14}	η_{th}	W_{pm}	m_{wf}	m_{cs}	Q_{PE}	Q_{Ev}	Q_{PC}	Q_{Cn}
	%	kW	kg.s^{-1}	kg.s^{-1}	MW	MW	MW	MW
0.0	11.12	32.4	23.6	230	4.4	6.8	1.5	8.4
0.1	11.49	29.9	22.9	230	4.4	6.8	1.5	8.4
0.2	11.70	27.4	22.5	229	4.4	6.8	1.5	8.3
0.3	11.80	25.2	22.2	229	4.4	6.8	1.6	8.3
0.4	11.83	23.1	22.0	229	4.4	6.8	1.6	8.3
0.5	11.83	21.2	22.0	229	4.3	6.8	1.6	8.3
0.6	11.78	19.4	22.0	229	4.3	6.9	1.6	8.2
0.7	11.66	17.6	22.2	229	4.3	6.9	1.6	8.3
0.8	11.52	16.0	22.4	229	4.2	7.0	1.6	8.3
0.9	11.33	14.4	22.8	230	4.1	7.1	1.6	8.3
1.0	11.10	12.8	23.4	231	4.0	7.2	1.6	8.3

The total heat inflow to the cycle (in all cases) is about 11.2 MW with roughly 60% – 65% used to evaporate the working fluids, while the rest is used for pre-heating the fluids to their bubble points. On average, about 9.9 MW is rejected from the cycles, with 85% of that rejected via the condensation of the working fluids. A working-fluid mixture with $X_{C6H14} = 0.4$ results in the cycle with the highest power output and thermal efficiency. The (pure) *n*-hexane cycle has the lowest power output, closely followed by the *n*-pentane cycle; their power outputs are 6.8% and 5.2%, respectively, lower than that of the optimal mixture.

The working-fluid mixtures with *n*-hexane fractions between 30 mol% and 60 mol% generally have the highest power outputs and also the lowest working-fluid flow-rates (from Table 2). This implies that they result in cycles with the highest energy densities (defined as $\dot{W}_{\mathrm{exp}}/\dot{m}_{\mathrm{wf}}$). The pure fluids have the highest mass flow-rates and (coupled with their lower outputs) thus have the lowest energy densities. Their energy densities are 11.8% (for *n*-pentane) and 12.56% (for *n*-pentane) lower than that of the optimal fluid mixture.

As expected, there are larger temperature glides in the condenser than in the evaporator (Figure 3); the temperature glides in both heat exchangers follow a parabolic profile reaching a maximum at the equimolar mixture. This does not directly correspond to the optimal mixture, but is reasonably close as the glide profiles roughly match the maximum power output profiles. Mixtures with the highest power outputs also have among the highest temperature glides. This suggests that mixtures with higher temperature glides may well be the optimal fluids. This may only hold true for closely related bi-component mixtures, since it has been suggested that mixtures with highly differing properties do not follow this trend [15,16]

The optimal evaporation and condensation pressures (Figure 2, RHS) reduce linearly from *n*-pentane to *n*-hexane. This is because the saturation pressures of *n*-pentane are higher than those of *n*-hexane at the same temperature since critical pressure of *n*-pentane is higher than that for *n*-hexane. Only *n*-pentane was condensed at above atmospheric conditions, others working fluids were condensed in vacuum. The pump duty (while being negligible in comparison to the expander output) also decreases linearly, mirroring the behaviour of the optimal evaporation pressure.

The volumetric flow-rates through the expander, $\dot{V}_{\mathrm{exp}}$ (Figure 4, LHS) are linear, increasing steadily from *n*-pentane to *n*-hexane due to the reduction in the saturation pressures during evaporation and condensation. The pressure ratio, PR, and expansion ratio, VR, (Figure 4, RHS) follow the same trends, with a minimum for *n*-pentane and a maximum at a 60 mol% mixture. The expander for the *n*-pentane cycle has the lowest volumetric flow-rate and expansion ratio, suggesting that it would be much smaller than the expanders for the mixtures, potentially leading to cost savings. Also, it would need a lower number of stages as volumetric expanders are produced with a fixed ratio. Pure *n*-hexane on the other hand would require a large expander while still producing the least power output.

On average, the mass flow-rate of the cooling water needed to condense the working fluids is 230 kg.s^{-1}. It should be noted that the cooling-water rates are over four times higher than the heat source rates and about ten times higher than the working-fluid mass flow-rates due to the low temperature change (10 °C) imposed on the cooling stream.

HEAT TRANSFER ANALYSIS OF OPTIMAL CYCLES

In the previous section we demonstrated the thermodynamic benefits of deploying working-fluid mixtures in ORCs, especially for cases when the heat source and sink profiles are constrained. As expected, there are working-fluid mixtures that realize higher power outputs and thermal efficiencies than both pure fluids as a result of the temperature glides during the phase change processes. The associated expansion and pressure ratios of such working-fluid mixtures are comparable to those of the pure working-fluids.

However, these results were derived purely from a thermodynamic perspective, the effects of such mixtures on the heat transfer processes in the heat exchangers, most especially the evaporator and the condenser, are yet to be highlighted. Experimental investigations have shown that working-fluid mixtures are likely to experience lower heat-transfer coefficients than pure fluids under similar conditions. Thus, it is imperative to investigate the consequences of selecting fluid mixtures on the heat transfer processes in an ORC system with a view to the sizing of the system components and the prediction of component costs.

Pump and expander costs depend on their power ratings, and expansion/compression volume and pressure ratios; these variables were derived from the thermodynamic optimization and thus need no further treatment. The costs for heat exchangers on the other hand are based on their heat-transfer areas, which cannot be obtained from thermodynamic calculations alone. Thus, appropriate heat transfer models are required for the heat exchangers to be sized.

Heat Exchanger Sizing

The heat addition process of the cycle is carried out in two heat exchangers: (1) the Pre-Evaporator (PE), used to pre-heat the working fluid from sub-cooled liquid to saturated liquid; and (2) the Evaporator (Ev), used to evaporate the working fluid to the saturated vapour state. Similarly, the heat rejection process of the cycle is carried out in two heat exchangers: (1) the Pre-Condenser (PC); and (2) the Condenser (Cn). Each of the four heat exchangers is modelled as a counter-current shell-and-tube exchanger constructed from carbon-steel, and is discretized into 100 (variable-sized) segments; details are given in Table 3. A typical segment is illustrated in Figure 5. In all heat exchangers, the working fluid is the tube-side fluid, while the heat source and sink streams are the shell-side fluids.

Table 3: Heat exchanger parameters

Shell & tube diameters	70 mm & 25 mm
Tube thickness, dx	5 mm
Tube thermal conductivity, k	51 W.m^{-1}.K^{-1} [24]

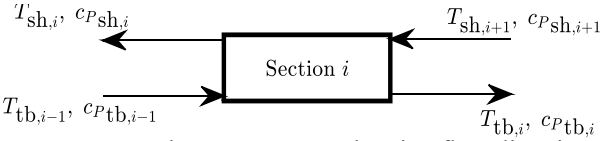

Figure 5 Heat exchanger segment showing flow directions on the shell (sh) and tube (tb) sides

Based on the set-up above, the total heat transferred to the working fluid and heat rejected from the working fluid in relation to Equations 2 and 4 respectively, are:

$$\dot{Q}_{\text{in}} = \dot{Q}_{\text{PE}} + \dot{Q}_{\text{Ev}} = \sum_{\text{i=1}}^{\text{ns,PE}} Q_{\text{i}} + \sum_{\text{i=1}}^{\text{ns,Ev}} Q_{\text{i}} \; ; \qquad [6]$$

$$\dot{Q}_{\text{out}} = \dot{Q}_{\text{PC}} + \dot{Q}_{\text{Cn}} = \sum_{\text{i=1}}^{\text{ns,PC}} Q_{\text{i}} + \sum_{\text{i=1}}^{\text{ns,Cn}} Q_{\text{i}} \; . \qquad [7]$$

An energy balance across each segment gives the heat transferred across the segment as:

$$\dot{Q}_{\text{i}} = \dot{m}_{\text{sh}}(T_{\text{sh,i+1}} c_{P_{\text{sh,i+1}}} - T_{\text{sh,i}} c_{P_{\text{sh,i}}}) = \dot{m}_{\text{tb}}(T_{\text{tb,i}} c_{P_{\text{tb,i}}} - T_{\text{tb,i-1}} c_{P_{\text{tb,i-1}}}) \; . \qquad [8]$$

Furthermore, for each segment an overall heat-transfer coefficient, U_{i} can be defined such that:

$$\dot{Q}_{\text{i}} = U_{\text{i}} A_{\text{i}} \Delta T_{\text{lm,i}} \; , \qquad [9]$$

where:

$$\Delta T_{\text{lm,i}} = \frac{(T_{\text{sh,i+1}} - T_{\text{tb,i}}) - (T_{\text{sh,i}} - T_{\text{tb,i-1}})}{\ln[(T_{\text{sh,i+1}} - T_{\text{tb,i}})/(T_{\text{sh,i}} - T_{\text{tb,i-1}})]} \; ; \qquad [10]$$

$$U_{\text{i}}^{-1} = h_{\text{sh,i}}^{-1} + \mathrm{d}x/k + h_{\text{tb,i}}^{-1} \; . \qquad [11]$$

Single-phase local heat-transfer coefficients (h_{sh} and h_{tb}) can be calculated by using the Dittus-Boelter correlation:

$$\text{Nu}_{i,\text{sp}} = 0.023 \text{Re}_i^{0.8} \text{Pr}_i^{\text{n}} \; , \qquad [12]$$

where $n = 0.4$ for a fluid being heated and $n = 0.3$ for a fluid being cooled, whereas two-phase heat-transfer coefficients can be calculated by suitably modifying Equation 12 with empirical functions of the Martinelli parameter [20,21]. This modification was fitted specifically to results from experiments involving horizontal turbulent-flow boiling of refrigerant mixtures:

$$\text{Nu}_{i,\text{tp}} = \text{F}(X_{\text{tt}}) \text{Nu}_{i,\text{sp}} \; , \qquad [13]$$

where:

$$\text{F}(X_{\text{tt}}) = 1 + 1.8 X_{\text{tt}}^{-0.82} \; ; \qquad [14]$$

$$X_{\text{tt}} = \left(\frac{1-q}{q}\right)^{0.9} \left(\frac{\rho_{\text{v}}}{\rho_{\text{l}}}\right)^{0.5} \left(\frac{\mu_{\text{l}}}{\mu_{\text{v}}}\right)^{0.1} \; . \qquad [15]$$

Equations 13-15 are applied directly for pure fluids using the overall mixture composition for the liquid and vapour phase properties. For the working-fluid mixtures, X_{tt} is calculated using the equilibrium liquid and vapour phase compositions (not the overall composition) at the saturation temperature and corresponding vapour quality (q, on mass basis) [20].

The heat-transfer areas of all segments are then calculated from Equation 9 and summed up to give the total heat-transfer area (A_{HX}) for the heat exchanger of interest:

$$A_{\text{HX}} = \sum_{i=1}^{ns} A_{\text{i}} \, , ns = 100 \; . \qquad [16]$$

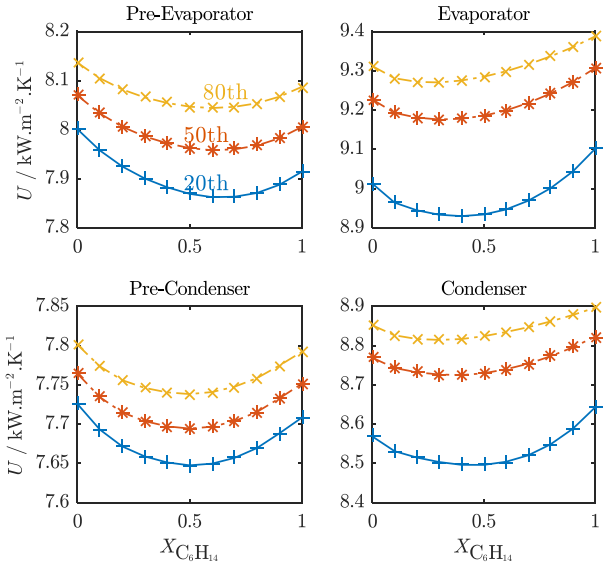

Figure 6: Overall heat-transfer coefficients at the 20th, 50th and 80th segments in the heat exchangers.

Heat Exchanger Sizing for Optimal Cycles

First, we verify the overall heat-transfer coefficients calculated using the set of Equations 11-15, especially for the heat exchangers involving phase change (Evaporator and Condenser). The overall heat-transfer coefficients at the 20th, 50th and 80th segments of these heat exchangers, including those for the single-phase heat exchangers, are presented in Figure 6. The calculated values are in general alignment with experimental data obtainable for flow boiling of refrigerant mixtures in Refs. [20,21].

Also in agreement with experimental observations, the heat-transfer coefficients for the working-fluid mixtures at each of the segments are lower than the linearly interpolated values between the two pure-fluid components that make up the mixture. While various explanations have been proposed for this phenomenon, most authors contend that it is due to mass transfer effects caused by the composition differences between vapour and liquid phases during phase change process.

In the single-phase heat exchangers (Pre-Evaporator and Pre-Condenser), the overall heat-transfer coefficients for the mixtures are also lower than the linearly interpolated values. Overall, the heat-transfer coefficients are highest in the Evaporator, followed by the Condenser and lowest in the Pre-Condenser. Higher heat-transfer coefficients are achieved in the Condenser and Evaporator due to the phase changes involved. The working-fluid vapour-phase results in the lower values in the Pre-Condenser.

With the knowledge of the heat-transfer coefficients and the associated heat transferred, the heat-transfer area for all segments of the heat exchangers are calculated from Equation 9. The heat-transfer areas of the segments in the Evaporator and the Condenser are presented in Figure 7. As the mole fraction of *n*-hexane is increased in the mixture, the heat-transfer area is seen to increase and then decrease such that the pure fluids (*n*-pentane and *n*-hexane) have heat exchangers with the lowest heat-transfer areas. This is the case across all the segments and in both the Evaporator and the Condenser.

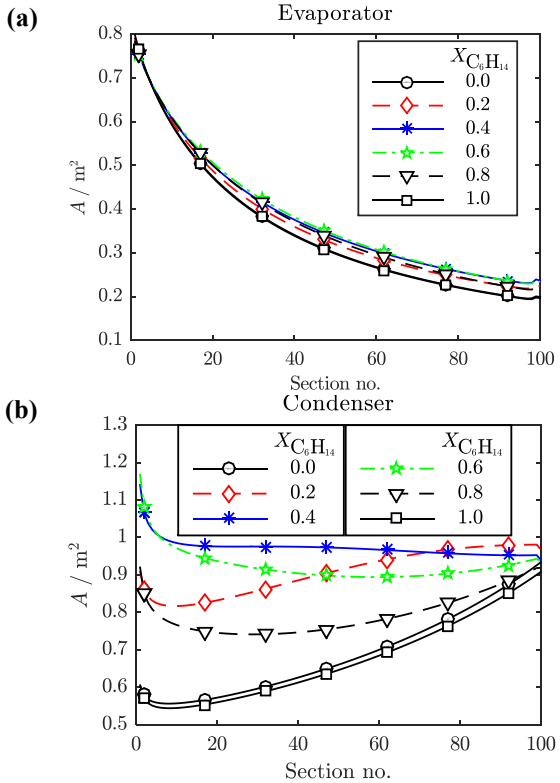

Figure 7: Heat-transfer areas along (a) Evaporator and (b) Condenser

Variations in the heat-transfer areas are less pronounced in Evaporator as opposed to the Condenser where large variations exist between the pure fluids and the mixtures. The pure working-fluids have the lowest areas across chiefly due to their higher values of heat-transfer coefficients. For example, even though the Evaporator for the case of pure *n*-hexane has the highest heat transferred amongst all Evaporators (see Table 2), it has the lowest areas because *n*-hexane results in the highest overall heat-transfer coefficients amongst all the working fluids.

The total heat-transfer areas for each of the heat exchangers with the different working-fluid mixtures from Equation 16 are presented in Figure 8 in normalized form. The areas are normalized (based on parameters in Table 4) with respect to:

$$A_{\mathrm{n}} = (A_{\mathrm{HX}} - A_{\mathrm{min}})/(A_{\mathrm{max}} - A_{\mathrm{min}}) \qquad [17]$$

The absolute total heat-transfer area gives a direct indication of the size of the heat exchanger, while the normalized form facilitates the comparison between the different fluid mixtures.

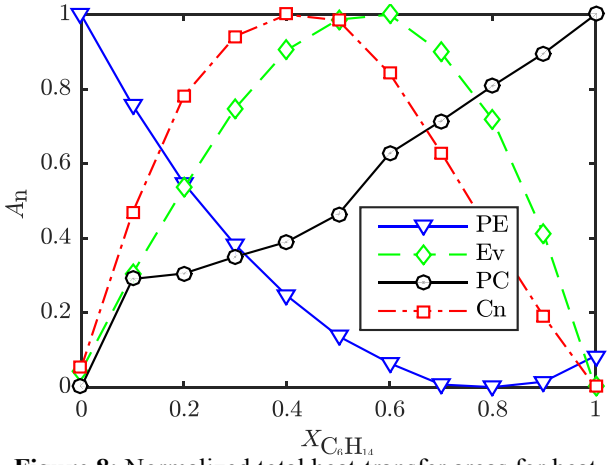

Figure 8: Normalized total heat-transfer areas for heat exchangers with the different working-fluid mixtures. Normalization parameters are given in Table 4

Table 4: Normalization parameters used in Equation 17

	PE	Ev	PC	Cn
A_{min} (m^2)	17.6	34.8	8.40	67.3
A_{max} (m^2)	19.6	38.3	8.60	97.3

As dictated by their thermal duties, the Evaporators are generally twice as large as the Pre-Evaporators while the Condensers are 8-10 times larger than the Pre-Condensers (see Table 2). Although the Condenser thermal duties are only about 15% higher than those of the Evaporators, the Condensers are twice as large as the Evaporators. This is due to the lower temperature differences across the Condensers.

As the concentration of *n*-hexane in the working-fluid mixture is increased, the heat duty of the Pre-Evaporator reduces and so does the total heat-transfer area of the Pre-Evaporator. The area reaches a minimum at 80 mol% *n*-hexane and then increases slightly for pure *n*-hexane. The opposite holds true for the Pre-Condenser with the heat duty and heat-transfer area increasing monotonically from *n*-pentane to *n*-hexane. The variations in heat-transfer area with working-fluid mixtures for the Pre-Evaporator and Pre-Condenser (range of 3.0 m^2 and 0.20 m^2 respectively) are much smaller than those associated with the two-phase heat exchangers. This suggests that the working-fluid mixtures have a more profound effect on the two-phase heat exchanger sizes than they do on the single-phase heat exchangers.

Furthermore, due to the deterioration of heat-transfer coefficients during phase change, the Evaporator and Condenser for the working-fluid mixtures are much larger than those for the pure fluids. This is especially true for the Condensers where the heat-transfer areas range from 67.3 m^2 ($X_{\mathrm{C6H14}} = 1$) to 97.3 m^2 ($X_{\mathrm{C6H14}} = 0.4$). Such large differences in heat-transfer areas between the working-fluid mixtures and the pure fluids could lead to sizeable differences in plant size and cost.

COST ANALYSIS OF OPTIMAL CYCLES

We conclude this paper with a brief investigation of the cost implications of employing working-fluid mixtures in ORC systems. The key components affected by the choice of working fluid are those illustrated previously – the working-fluid pump, the expander and the heat exchangers. The costs of these components are added to give an estimate of the plant cost. Although this sum does not give the total installation cost, it is through this amount that the effects of working fluid choice on plant costs are manifested directly. By and large, other factors that contribute to the plant installation costs would be similar for the other working fluids considered.

Component-base costs (C_{B}) are calculated using logarithmic correlations of component size factors (S):

$$C_{\mathrm{B}} = (\mathrm{F})\exp\{C_0 + C_1\,[\ln(S)] + C_2[\ln(S)]^2\}\ , \qquad [18]$$

where the size factors for the components considered are given in Table 5. Also in Table 5 are the cost coefficients, which have been derived from Seider *et al.*, 2010 [25] (the original coefficients have been converted to SI units). The calculated component-base costs of the optimal cycles are presented in Figure 9.

Table 5: Component cost coefficients used in Equation 18

Component	S	F	C_0	C_1	C_2
Pump	$\dot{V}\sqrt{H}$ ($m^3.s^{-1}.m^{1/2}$)	2.7	9.0073	0.4636	0.0519
Expander	W_{exp} (kW)	1.0	6.5106	0.8100	0.0000
Expander*	W_{exp} (kW)	1.0	7.3194	0.8100	0.0000
Heaters/ Coolers	A (m^2)	1.0	10.106	-0.4429	0.0901
Evaporator/ Condenser	A (m^2)	1.0	9.5638	0.5320	-0.0002

* Vacuum discharge expander (applicable to $X_{\mathrm{C6H14}} \geq 0.1$)

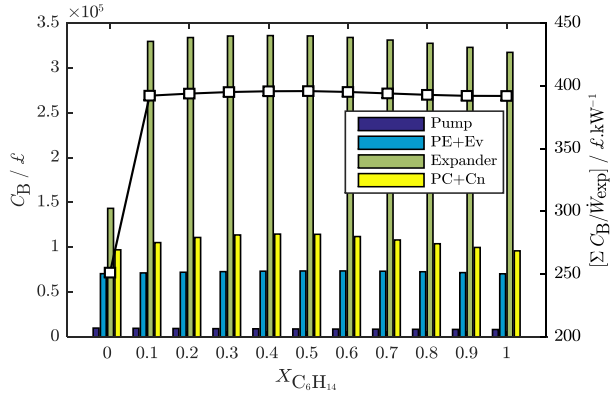

Figure 9: Optimal cycles' component costs and cost per kW

The working-fluid pumps cost around £ 9,000, with the cost reducing monotonically from *n*-pentane to *n*-hexane. This is a direct result of the lower evaporation pressures as the concentration of *n*-hexane in the working fluid is increased (see Figure 2). Similarly, the costs of the single-phase heat exchangers (Pre-Evaporator and Pre-Condenser) are low (between £ 9,300 and £ 9,500). However, the evaporator, condenser and expander cost are well in excess of £ 50,000.

From this result, it is clear that the expanders and the phase-change heat exchangers present the dominant costs of the ORC

system. The pure working-fluids generally have the lowest-cost evaporators and condensers, while the fluid mixtures ($X_{C6H14} = 0.6$ and $X_{C6H14} = 0.4$, respectively) have the highest costs. The condenser size and cost is smallest for *n*-pentane despite it having a larger heat duty and working-fluid flow-rate (see Table 2) than those for the mixtures. Thus the expander costs mirror the trend exhibited by the optimal power output in Figure 2. The exception to this is that of pure *n*-pentane ($X_{C6H14} = 0$) working fluid in which the expander cost over 50% lower than those of the other working fluids. After expansion, the *n*-pentane vapour exits the expander at above atmospheric pressure while all the other fluids exit at sub-atmospheric pressures and had their expander costs calculated with the vacuum discharge expander correlation in Table 5. This in turn makes the *n*-pentane expander cheaper than the rest.

Finally, we complete the cost analysis by considering the 'rated costs' for the optimal cycles, *i.e.*, cost per kilowatt of power generated ($\sum C_B / \dot{W}_{exp}$). This is done such that high power output fluids (especially the fluid mixtures) are not unnecessarily penalized. The rated costs of the optimal cycles are also plotted in Figure 9 (RHS). As expected, the ORC system with *n*-pentane as the working fluid has the lowest rated cost (£ 252/kW) due to its very low expander cost compared to the other working fluids. The cycle with *n*-hexane as the working fluid has the second lowest rated cost at £ 392/kW, whereas the cycle with $X_{C6H14} = 0.5$ has the highest rated cost at £ 396/kW. The previously identified, thermodynamically optimal fluid mixture ($X_{C6H14} = 0.4$; see Figure 2) also has a cycle rated cost of £ 396/kW. On the other hand, the cost optimal working fluid is *n*-pentane, which gives a rated cost reduction of 37% over the thermodynamically optimal working fluid.

CONCLUSIONS

This aim of this study was to investigate the thermodynamic benefits of employing working-fluid mixtures in organic Rankine cycle (ORC) systems and the effects of selecting such mixtures on the sizes and costs of ORC engines. We use *n*-pentane and *n*-hexane, and their mixtures, for this investigation due to the common use of the former in ORC installations. A geothermal-type, hot-water heat-source stream was used. The analyses reveal that the temperature glides of the working-fluid mixtures during evaporation and condensation result in higher power output and thermal efficiencies for fluid mixtures with the mixture containing 40 mol% of *n*-hexane having the highest output, more than either pure fluids. The pure fluids do however result in smaller sized expanders due to their low volumetric flow-rates and low expansion ratios. The working-fluid mixtures were seen to have the largest evaporators and condensers. Thus, they required more expensive heat exchangers when compared to the pure fluids.

Moreover, due to the sub-atmospheric expansion, the expander costs in the case of the working-fluid mixtures (and pure *n*-hexane) were much higher than that for pure *n*-pentane. Generally, equipment sizes and costs are larger for the mixtures than for the pure fluids. Thus, the working-fluid mixtures would require a larger plant layout area, contributing significantly to the overall installation costs.

Although the mixtures have the highest power output, they also have the highest rated cost (equipment cost per kilowatt power generated). On the other hand, ORC systems with pure *n*-pentane working have the lowest rated cost followed by those with *n*-hexane. These imply that the thermodynamic benefits derived from using the working-fluid mixtures are not suitably justified by the increased cost incurred. This underlines the importance of heat transfer and cost analyses in the selection of optimal working-fluid (mixtures) for ORC systems.

REFERENCES

[1] Angelino G., and Colonna Di Paliano P., Multicomponent Working Fluids for Organic Rankine Cycles (ORCs), *Energy*, Vol. 23, 1998, pp. 449-463

[2] Garg P., Kumar P., Srinivasan K., and Dutta P., Evaluation of Isopentane, R-245fa and Their Mixtures as Working Fluids for Organic Rankine Cycles, *Applied Thermal Engineering*, Vol. 51, 2013, pp. 292-300

[3] Wang J.L., Zhao L., and Wang X.D., A Comparative Study of Pure and Zeotropic Mixtures in Low-Temperature Solar Rankine Cycle, *Appl. Energy*, Vol. 87, 2010, pp. 3366-3373

[4] Van Den Broeck M., Chys M., Vanslambrouck B., and De Paepe M., Increasing the Efficiency and Generated Electricity of Organic Rankine Cycles by using Zeotropic Mixtures as Working Fluids, *Energy*, Vol. 44, 2012, pp. 623-632

[5] Sami S.M., Energy and Exergy Analysis of New Refrigerant Mixtures in an Organic Rankine Cycle for Low Temperature Power Generation, *International Journal of Ambient Energy*, Vol. 31, 2010, pp. 23-32

[6] Chen H., Goswami D.Y., Rahman M.M., and Stefanakos E.K., A Supercritical Rankine Cycle using Zeotropic Mixture Working Fluids for the Conversion of Low-Grade Heat into Power, *Applied Thermal Engineering*, Vol. 36, 2011, pp. 549-555

[7] Zhao L., and Bao J., Thermodynamic Analysis of Organic Rankine Cycle using Zeotropic Mixtures, *Applied Energy*, *130*, 2014, pp. 748-756

[8] Aghahosseini S., and Dincer I., Comparative Performance Analysis of Low-Temperature Organic Rankine Cycle (ORC) using Pure and Zeotropic Working Fluids, *Applied Thermal Engineering,* 54, 2013, pp. 35-42

[9] Heberle F., Preißinger M., and Brüggemann D., Zeotropic Mixtures as Working Fluids in Organic Rankine Cycles for Low-Enthalpy Geothermal Resources, *Renewable Energy*, Vol. 37, 2012, pp. 364-370

[10] Shu G., Gao Y., Tian H., Wei H., and Liang X., Study of Mixtures based on Hydrocarbons used in ORC (Organic Rankine Cycle) for Engine Waste Heat Recovery, *Energy*, *74*, 2014, pp. 428-438.

[11] Lecompte S., Ameel B., Ziviani D., van den Broek M., and De Paepe M., Exergy Analysis of Zeotropic Mixtures as Working Fluids in Organic Rankine Cycles, *Energy Conversion and Management*, Vol. 85, 2014, pp. 727-739

[12] Chys M., van den Broek M., Vanslambrouck B., and De Paepe M., Potential of Zeotropic Mixtures as Working Fluids in Organic Rankine Cycles, *Energy*, *44*, 2012, pp. 623-632

[13] Braimakis K., Leontaritis A., Preißinger M., Karellas S., Brüggeman D., and Panopoulos K., Thermodynamic Investigation of Waste Heat Recovery with Subcritical and Supercritical Low-Temperature Organic Rankine Cycle based on Natural Refrigerants and their Binary Mixtures, *Proceedings of the 27th International Conference on Efficiency, Cost, Optimization, Simulation and Environmental Impact of Energy Systems,* 2014

[14] Dong B., Xu G., Cai Y., and Li H., Analysis of Zeotropic Mixtures used in High-Temperature Organic Rankine Cycle, *Energy Conversion and Management*, *84*, 2014, pp. 253-260

[15] Li Y. R., Du M. T., Wu C. M., Wu S. Y., and Liu C., Potential of Organic Rankine Cycle using Zeotropic Mixtures as Working Fluids for Waste Heat Recovery, *Energy*, *77*, 2014, pp. 509-519

[16] Oyewunmi O. A., Taleb A. I., Haslam A. J., and Markides C. N., An assessment of working-fluid mixtures using SAFT-VR Mie for use in organic Rankine cycle systems for waste-heat recovery, *Computational Thermal Sciences,* Vol. 6, 2014, 301-316

[17] Lampe M., Stavrou M., Bücker H. M., Gross J., and Bardow A., Simultaneous Optimization of Working Fluid and Process for Organic Rankine Cycles Using PC-SAFT, *Applied Thermal Engineering*, Vol. 53, 2014, pp. 8821-8830

[18] Papadopoulos A. I., Stijepovic M., and Linke P., On the Systematic Design and Selection of Optimal Working Fluids for Organic Rankine Cycles, *Applied Thermal Engineering*, Vol. 30, 2010, pp. 760-769

[19] Papadopoulos A. I., Stijepovic M., Linke P., Seferlis P., and Voutetakis S., Toward Optimum Working Fluid Mixtures for Organic Rankine Cycles using Molecular Design and Sensitivity Analysis *Applied Thermal Engineering*, Vol. 52, 2013, pp. 12116-12133

[20] Jung D.S., McLiden M., Radermacher R., and Didion D., Horizontal Flow Boiling Heat Transfer Experiments with a Mixture of R22/R114, *International Journal of Heat and Mass Transfer*, Vol. 32, 1989, pp. 131-145

[21] Shin J.Y., Kim M.S., and Ro S.T., Correlation of Evaporative Heat Transfer for Refrigerant Mixtures, *International Refrigeration and Air Conditioning Conference,* 1996, pp. 316

[22] Kunz O., and Wagner W., The GERG-2008 Wide-Range Equation of State for Natural Gases and Other Mixtures: An Expansion of GERG-2004, *Journal of Chemical Engineering Data*, Vol. 57, 2012, pp. 3032-3091

[23] Byrd R.H., Mary E.H., and Jorge N., An Interior Point Algorithm for Large-Scale Nonlinear Programming, SIAM Journal on Optimization, *SIAM Journal on Optimization*, Vol. 9, 1999, pp. 877–900

[24] The Engineering Toolbox http://www.engineeringtoolbox.com/ thermal-conductivity-d_429.html. Accessed 11/01/2015.

[25] Seider W.D., Seader J.D., and Lewin D.R., *Product and Process Design Principles*, New York: Wiley, 2004. Print